Composites Part B 205 (2021) 108510

Contents lists available at ScienceDirect

Composites Part B

journal homepage: www.elsevier.com/locate/compositesb

UV resistant PBT nanocomposites by reactive compatibilization and selective distribution of tailor-made double-shelled TiO_2 nanohybrids

Ying Cao [a], Pengwu Xu [a], Weijun Yang [a], Xiangmiao Zhu [a], Weifu Dong [a], Mingqing Chen [a], Mingliang Du [a], Tianxi Liu [a], Pieter Jan Lemstra [a,b], Piming Ma [a,*]

[a] The Key Laboratory of Synthetic and Biological Colloids, Ministry of Education, Jiangnan University, 1800 Lihu Road, Wuxi, 214122, China
[b] PlemPolco B.V., De Zicht 11, 5502, HV Veldhoven, the Netherlands

ARTICLE INFO

Keywords:
Poly (butylene terephthalate)
Nanocomposites
Toughness
UV resistance

ABSTRACT

The application and service life of poly (butylene terephthalate) (PBT) is limited by its brittleness and ultraviolet (UV) instability. Titanium dioxide (TiO_2) in PBT matrix can shield for UV light, but it triggers further photo-degradation of PBT via a photocatalytic effect. In this work, both toughness and against prolonged UV radiation of PBT from recycled source are significantly improved by reactive compounding with ethylene-vinyl acetate-glycidyl methacrylate copolymer (EVMG) and tailor-made double-shelled TiO_2@SiO_2-g-EVMG nanohybrids. The inner SiO_2 shell prevents direct contact of TiO_2 and the PBT matrix, while the grafted EVMG outer shell promotes a selective distribution and uniform dispersion of TiO_2 in the EVMG phase only. Consequently, the impact toughness of PBT/EVMG/TiO_2@SiO_2-g-EVMG nanocomposites is 18 times higher than that of neat PBT. Moreover, the tensile strength and the elongation at break of the nanocomposites remain 95% and 87% respectively after 48-h accelerated UV irradiation. Meanwhile, 90% UV light can be shielded by the PBT/EVMG/TiO_2@SiO_2-g-EVMG nanocomposites. Therefore, this work provides a facile route to make PBT nanocomposites with superior mechanical and UV resistant performances, which may broaden the application range of (recycled) PBT and e.g. PBT/Polycarbonate blends.

1. Introduction

Poly (butylene terephthalate), i.e. PBT, is used successfully in automotive and electronic parts, and some other fields due to its high strength, excellent electrical insulation properties and good process characteristics. However, PBT is brittle and shows a notched impact strength of only 4 kJ/m^2.[1–3]. Meanwhile, PBT materials and products thereof are prone to undergo aging and degradation in long-term sunlight irradiation, because free radicals generated after UV irradiation could break the molecular chains, resulting in deterioration in mechanical properties [4–6]. Thus, improving the toughness and UV resistance is of importance for the safety and service life of PBT-based materials and products made thereof.

Compounding with elastomers is a simple and efficient method to improve the toughness of plastics. Based on this fact, reactive compatibilization [7–10], dynamic vulcanization [11–14], nano-technology [15–21] etc. have been used to further enhance the toughening effect of elastomers and even endow polymers with special functions. For example, Li et al. [15] introduced maleic anhydride grafted styrene-ethylene-butylene-styrene (SEBS-g-MAH) copolymer and carbon nanotubes (CNTs) into polycarbonate (PC)/PBT blends, which lead to a great enhancement in the toughness from 4.8 to 43 kJ/m^2 and a formation of percolated conductive network structure. Huang et al. [22] designed polylactide (PLA)/epoxidized natural rubber (ENR)/Fe_3O_4 thermoplastic vulcanizates (TPVs) with a better compatibility between PLA and ENR by dynamic vulcanization, achieving an increase by 16 times in toughness and excellent self-healing behaviour. Thus, brittleness of some polymers can be conquered by tuning the compatibility between polymer matrix and elastomer phase, and sometimes with the synergistic effect of introducing functionalities such as electrical conducting and self-healing. However, toughening modification in combination with UV-shielding and UV resistance to PBT-based materials have not been well studied yet.

TiO_2 has been widely used in the fields of photo-catalysis and UV-shielding due to its inherent peculiarity of shielding from UV light, which have been reported in various nanocomposite systems, such as

* Corresponding author.
E-mail address: p.ma@jiangnan.edu.cn (P. Ma).

https://doi.org/10.1016/j.compositesb.2020.108510
Received 7 September 2020; Received in revised form 18 October 2020; Accepted 2 November 2020
Available online 11 November 2020

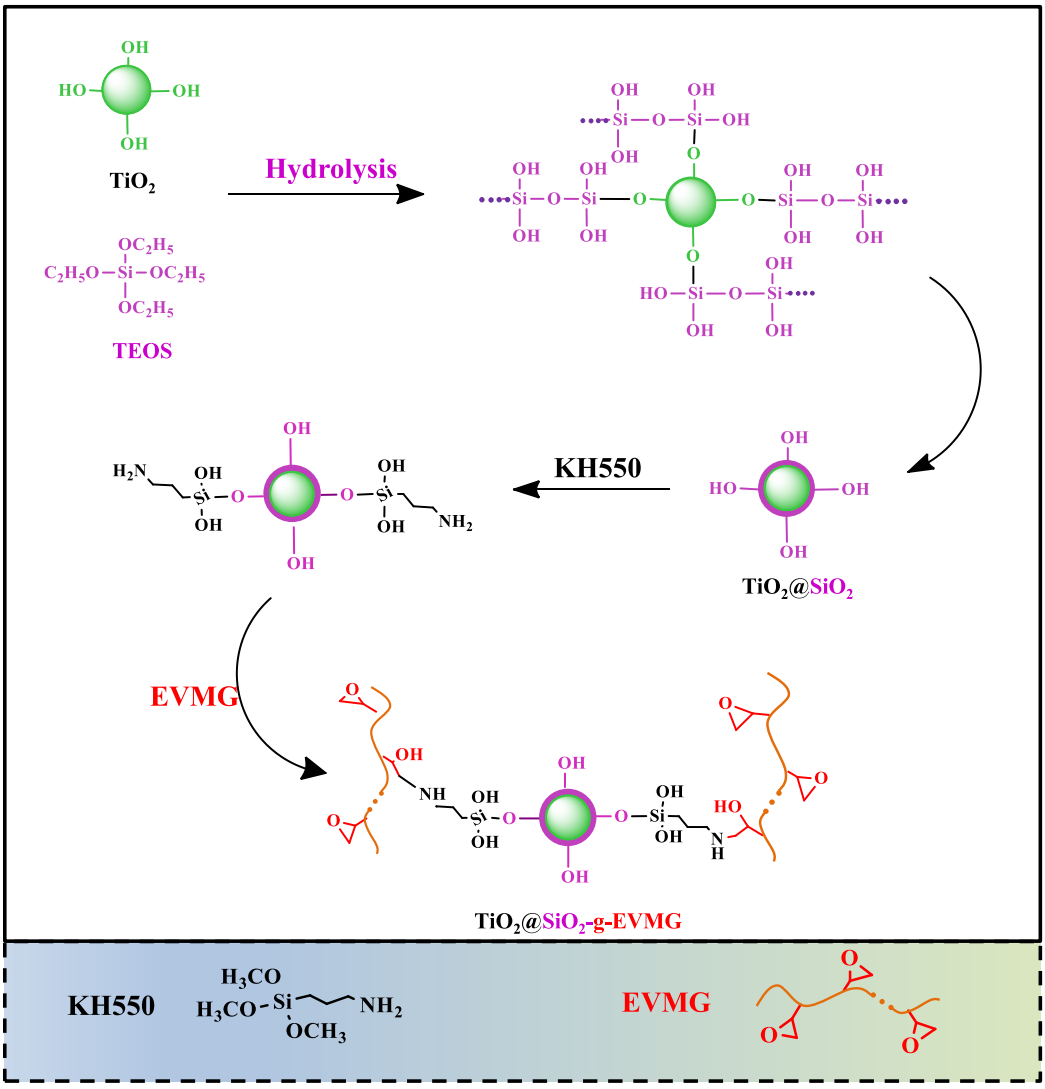

Scheme 1. Schematic diagram of the synthesis of TiO_2@SiO_2-g-EVMG nanohybrids.

PLA/TiO_2 [23,24], polyamide/TiO_2[25], TiO_2@fabrics [26,27], silk/-TiO_2 [28] and polypropylene/TiO_2 [29] etc. Huang et al. [26] designed the TiO_2@fabric nanocomposite via a one-pot hydrothermal reaction, leading to 12 times increase in ultraviolet protection factor. However, the addition of TiO_2 usually leads to severe degradation of polymeric materials due to its active oxygen species under UV irradiation [30]. Zan et al. [31] prepared polyethylene/TiO_2 nanocomposite films, however the film degraded significantly under UV or sunlight irradiation. Buzarovska et al. [32] found that the degradation rate of PLA was increased by 15 times after incorporation of even a small amount of 1.0 wt% TiO_2 nanoparticles. The degradation consequently deteriorated mechanical properties of the corresponding materials. Hence, it is still challenging to prepare polymer/TiO_2 nanocomposites with both UV-shielding property and UV resistance.

The primary objective of this work is to design PBT-based (nano) composites including from recycled sources possessing toughness, UV-shielding and UV resistance by incorporation of ethylene-vinyl acetate-glycidyl methacrylate copolymer (EVMG) and tailor-made double-shelled TiO_2@SiO_2-g-EVMG nanohybrids. The inner SiO_2-shell was designed to keep active oxygen species of TiO_2 under UV irradiation away from the PBT matrix, while the grafted EVMG chains were designed to make TiO_2@SiO_2-g-EVMG selectively and uniformly distribute in the EVMG phase to further weaken the photocatalytic effect of TiO_2. Therefore, this study provides a new design and a facile route for preparing super-tough PBT-based nanocomposites with both UV-shielding and UV resistance properties, which may broaden the application range of PBT and even other polyester materials as engineering and durable plastics.

It is worth to note that this work uses recycled PBT as a raw material, thus it also provides a potential solution for solving environmental issues such as CO_2 emission, plastic waste and marine micro-plastics.

2. Experiments

2.1. Materials

Recycled-PBT with a melt flow rate of 27.4 g/10min (250 °C/2.16 kg) and melting temperature of 223 °C was provided by Dongguan Zhangmutou Co., Ltd. Epoxidized elastomer, i.e., ethylene-vinyl acetate-glycidyl methacrylate copolymer (EVMG) containing 60 wt% of vinyl acetate and 0.022 mol epoxy groups per 100 g was supplied by Arlanxeo Deutschland GmbH. TiO_2 (purity > 99.8%) was purchased from Shanghai Maclean Biochemical Technology Co., Ltd. Silane coupling agent (3-triethoxysilylpropylamine, KH550, 98%), tetraethyl orthosilicate (TEOS, AR), N,N-dimethylformamide (DMF, AR), ammonium hydroxide ($NH_3{\cdot}H_2O$, AR) sodium hexametaphosphate (AR), ethanol and

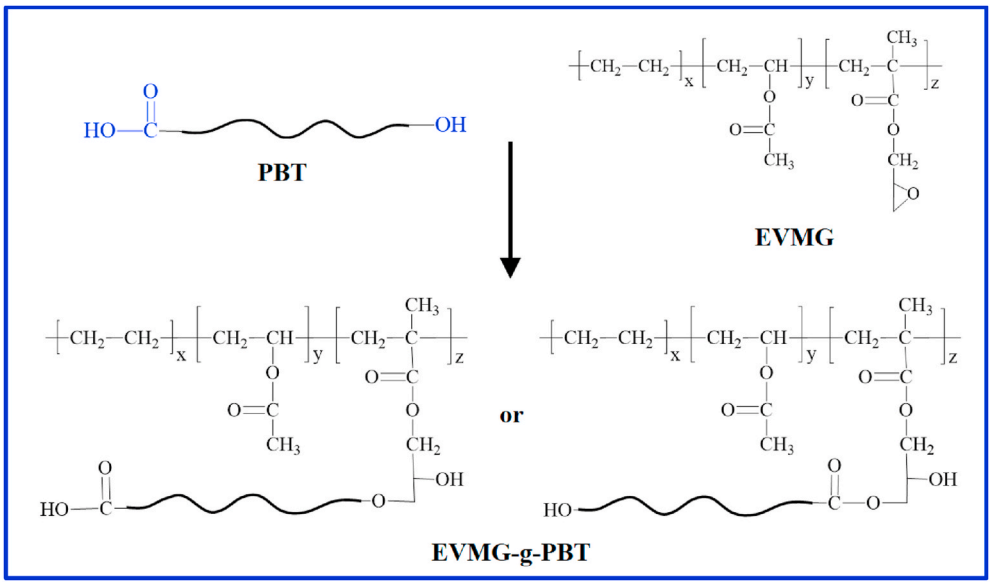

Scheme 2. The possible reactions between the PBT matrix and the EVMG.

chloroform were all obtained from Sinopharm Group Co., Ltd.

2.2. Preparation of TiO_2@SiO_2-g-EVMG nanohybrids

TiO_2@SiO_2 nanoparticles were first prepared through the hydrolysis of TEOS on the surface of TiO_2. The well-known Silane coupling agent KH-550 (3-Aminopropyltriethoxysilane) was used to obtain the TiO_2@SiO_2–KH550 nanohybrids. Subsequently, TiO_2@SiO_2-g-EVMG nanohybrids were obtained by grafting EVMG onto TiO_2@SiO_2–KH550 nanoparticles via the reaction between the amino groups of KH550 and the epoxy groups of EVMG. The schematic diagram of the preparation process is shown in Scheme 1. The experimental details are provided in supporting information.

2.3. Preparation of PBT/EVMG/TiO_2@SiO_2-g-EVMG nanocomposites

PBT/EVMG/TiO_2@SiO_2-g-EVMG nanocomposites with different TiO_2@SiO_2-g-EVMG contents (0.3, 0.7, 1.0 and 2.0 wt%) were prepared by a Polylab-OS mixer (Haake, Germany) with a rotor speed of 80 rpm at 235 °C for 8 min. The samples were denoted as P/E/T-E_x, wherein the P, E and T-E represent PBT, EVMG and TiO_2@SiO_2-g-EVMG, respectively. A mixture of the PBT and the EVMG with a weight ratio of 80/20 was used. The x represents the weight percentage of TiO_2@SiO_2-g-EVMG in the nanocomposites. For comparison, PBT/EVMG/TiO_2 nanocomposites were prepared in the same way and denoted as P/E/T_x. Specimens for different measurements were prepared by hot compression molding at 240 °C and 10 MPa. The possible reactions between the PBT matrix and EVMG were shown in Scheme 2. The terminal carboxy group and the terminal hydroxyl group from the PBT matrix can react with the epoxy group from EVMG to form PBT-EVMG copolymer.

2.4. Characterization

Transmission electron microscopy (TEM). The morphology of TiO_2, TiO_2@SiO_2 nanoparticles and PBT nanocomposites were observed by TEM (JEM-2100plus, Japan) at an accelerating voltage of 200 kV. Specifically, TiO_2 and TiO_2@SiO_2 nanoparticles were ultrasonically dispersed in ethanol with a concentration of 0.5 mg/mL. And then, 5 μL TiO_2 and TiO_2@SiO_2 suspension were dropped on the copper net and observed after ethanol volatilizing. The PBT nanocomposites were microtomed to an ultrathin section (~80 nm in thickness) at −120 °C before observing.

Photocatalytic activities. The photocatalytic activities of TiO_2 and TiO_2@SiO_2 nanoparticles were characterized on a double beam UV–Vis spectrophotometer (TU-1901, China) by tracking the decomposition of rhodamine B solution (10 mg/L) with TiO_2 or TiO_2@SiO_2 nanoparticles (50 mg). The UV lamp with a wavelength of 330 nm and a power of 300 W was used for UV irradiation. Samples were taken from the solution every half hour and the supernatant without any nanoparticles after centrifuging was taken for testing.

Scanning electron microscopy (SEM). The surface morphology of PBT nanocomposites before and after UV irradiation was observed by SEM (S-4800, Japan) at an accelerating voltage of 3 KV. All the samples were sputtered with a thin golden layer before observation.

Fourier transform infrared (FT-IR). The TiO_2, TiO_2@SiO_2 and TiO_2@SiO_2-g-EVMG nanohybrids were analyzed using FT-IR spectrometer (Nicolet 6700, US) in attenuated total reflection mode (ATR). The final spectrum of each sample was an average of 32 scans at a resolution of 4 cm^{-1} in the wavenumber range of 400–4000 cm^{-1}.

Thermogravimetric analysis (TGA). The decomposition behaviour of TiO_2, TiO_2@SiO_2 and TiO_2@SiO_2-g-EVMG nanohybrids was detected by a TGA instrument (1100SF, Switzerland) from 50 to 600 °C at 10 °C/min in a nitrogen atmosphere.

X-ray diffraction (XRD). The crystal structures of TiO_2, TiO_2@SiO_2 and TiO_2@SiO_2-g-EVMG nanohybrids were analyzed by an X-ray diffractometer (Bruker AXS D8, Germany), wherein the 2-theta scan range was 5–90° and the scanning speed was 3°·min^{-1}.

Energy dispersive spectroscopy (EDS). The EDS line scanning and elemental analysis results of TiO_2 and TiO_2@SiO_2 nanoparticles were obtained on SEM (S-4800, Japan) with an accelerating voltage of 10 KV.

Mechanical properties. The tensile properties of PBT nanocomposites before and after UV irradiation (330 nm, 300 W) were measured using a tensile tester (Instron 5967, USA) and the notched Izod impact tests were carried out according to ISO 180 using an impact tester at room temperature. Five measurements of each sample were performed and the averaged values were presented.

UV-shielding properties. The UV absorption spectra of PBT nanocomposites were obtained on an UV–Vis near-infrared spectrophotometer (UV-3600, Japan) with an integrating sphere to evaluate the UV-shielding properties of the nanocomposites. The spectrum of each sample was presented in the wavelength range of 200–500 nm.

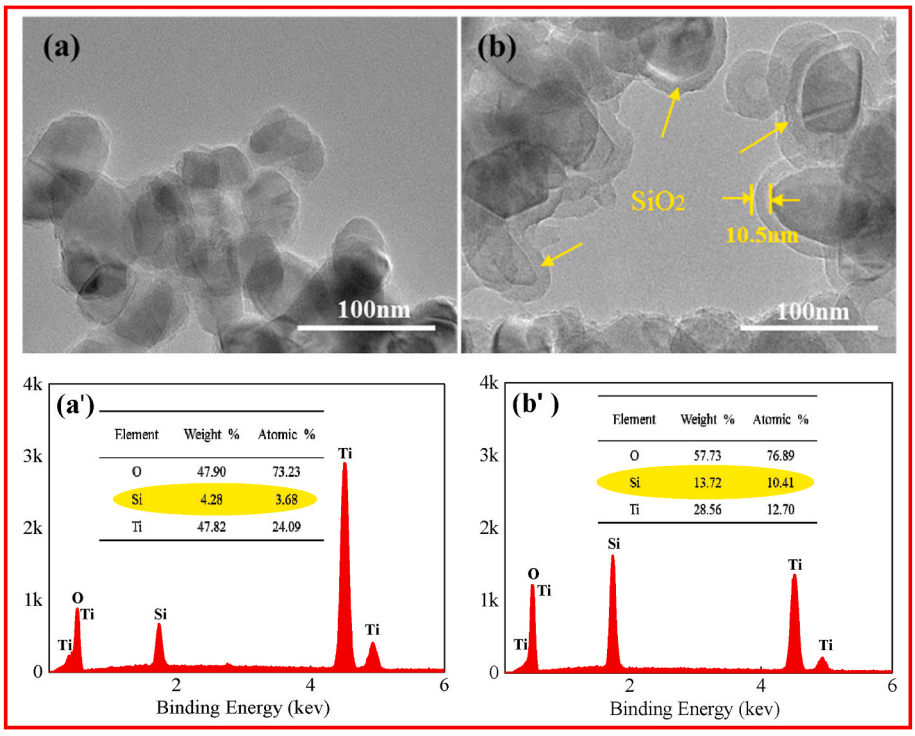

Fig. 1. TEM images and EDS spectra of (a/a') TiO_2 and (b/b') TiO_2@SiO_2 nanoparticles.

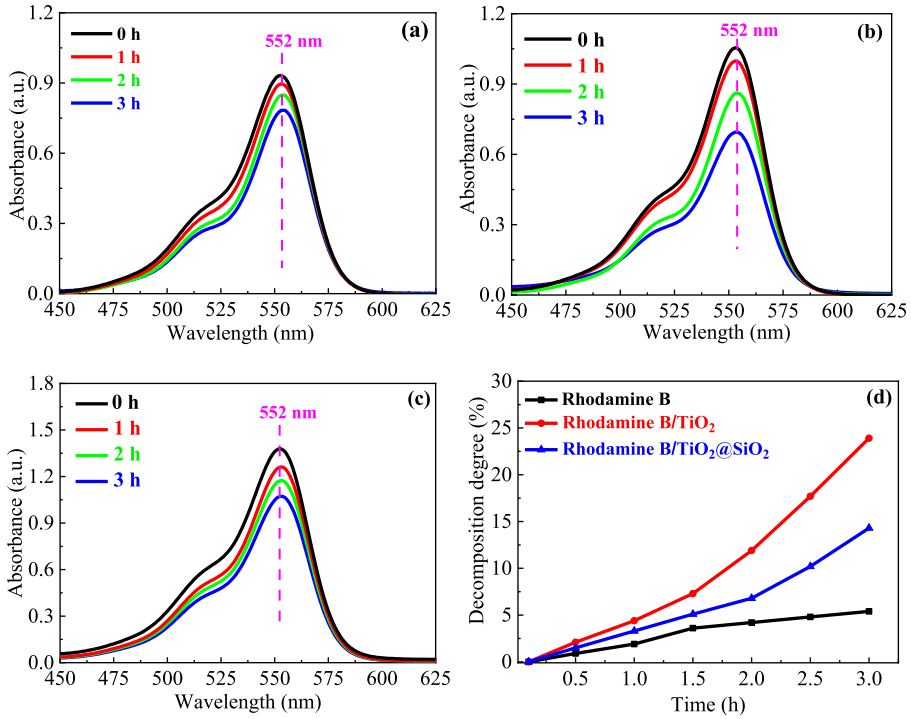

Fig. 2. UV absorption spectra of rhodamine B solutions after UV irradiation from (a) rhodamine B, (b) rhodamine B/TiO_2, (c) rhodamine B/TiO_2@SiO_2 samples, (d) decomposition degree of rhodamine B in different samples. Samples were taken from the corresponding solution and the supernatant without nanoparticles after centrifuging was taken for test.

3. Results and discussion

3.1. TiO_2@SiO_2 core-shell structure analysis and photocatalytic activity

The morphology of TiO_2 and TiO_2@SiO_2 was observed by TEM, as shown in Fig. 1a–b, respectively. It is clearly observed that TiO_2 nanoparticles show irregular shapes with a size of 50–100 nm (Fig. 1a), while TiO_2@SiO_2 nanoparticles present typical core-shell structures with a shell thickness of around 10 nm (Fig. 1b). The shell can be assigned to the SiO_2 layer. The TEM results confirmed that the TiO_2@SiO_2

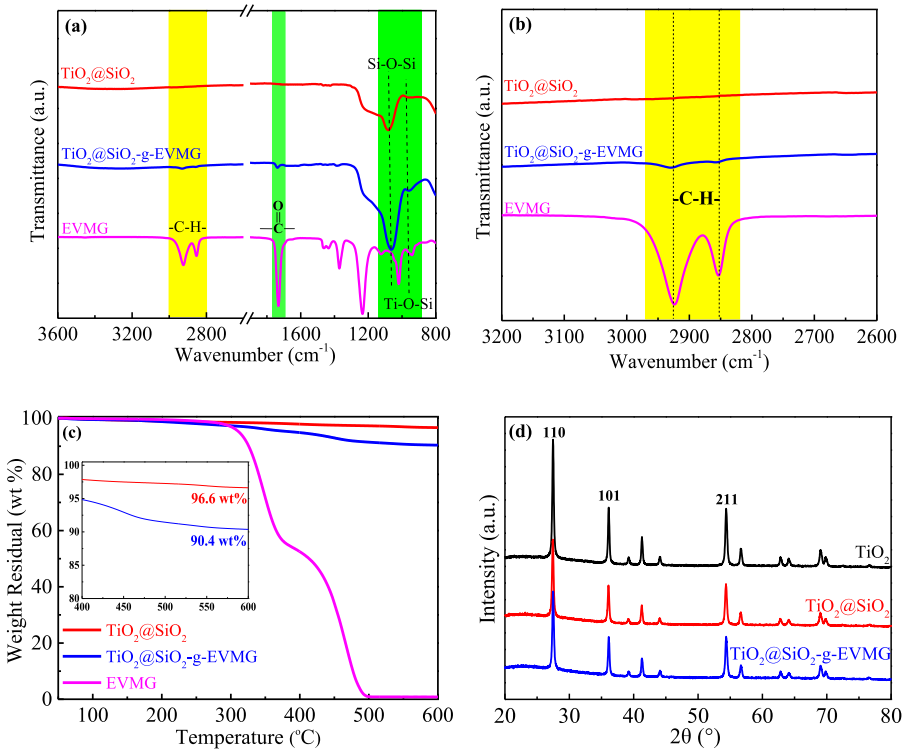

Fig. 3. (a, b) FT-IR spectra, (c) TGA curves of TiO_2@SiO_2, TiO_2@SiO_2-g-EVMG and EVMG, and (d) XRD patterns of TiO_2, TiO_2@SiO_2 and TiO_2@SiO_2-g-EVMG.

nanoparticles with the core-shell structure were achieved. Such a structure of TiO_2@SiO_2 nanoparticles is further confirmed by elemental analysis for TiO_2 and TiO_2@SiO_2 using energy dispersive spectroscopy (EDS), as shown in Fig. 1a'/1b'. The authors hasten to remark that the Si signal was also detected in neat TiO_2 sample which was due to the organic treatment during preparation process at the manufacturer. However, the content of Si element for TiO_2@SiO_2 nanoparticles is considerably higher in comparison with neat TiO_2, indicating that SiO_2 was indeed coated on the surface of TiO_2 nanoparticles.

The coating of SiO_2 is designed to reduce or ideally prevent the photocatalytic effect of TiO_2 on the degradation of PBT under UV irradiation. Therefore, the photocatalytic activities of TiO_2 and TiO_2@SiO_2 nanoparticles were evaluated by tracing the decomposition of rhodamine B, and the decomposition degree of rhodamine B could be quantitative by the following formula:

$$\text{Decomposition degree} = \frac{A_0 - A_t}{A_0} \times 100\%$$

where, A_0 and A_t is the UV absorption value of the rhodamine B solution at the wavelength of 552 nm before and after UV irradiation, respectively [33]. The UV absorption spectra and the results of decomposition degree calculated are shown in Fig. 2.

As expected, the absorption peak of rhodamine B at 552 nm is getting weak with the UV irradiation time (Fig. 2a) due to the gradual decomposition of rhodamine B. It is known that electrons (e^-_{cb}) in TiO_2 nanoparticles could absorb energy and jump from the valence band to the conduction band with UV light, thus leaving holes (h^+_{vb}) in the valence band. The electrons on the guide band can react easily with O_2 forming $\bullet O_2$, while the holes can easily react with H_2O to form •OH. The $\bullet O_2$ and •OH with high chemical activity can cleave organics into H_2O and O_2 during the contacting process [34,35]. Therefore, the absorption peak of rhodamine B at 552 nm reduced much faster after incorporation of TiO_2 because of its photocatalytic activity (Fig. 2b). On the other hand, the SiO_2-shell on the surface of TiO_2 effectively decreased the decomposition rate of rhodamine B because of the shielding layer between TiO_2 and rhodamine B. Consequently, the decomposition rate of rhodamine B composites is in the order of rhodamine B/TiO_2 > rhodamine B/TiO_2@SiO_2 > rhodamine B, as shown in Fig. 2d.

3.2. Chemical and crystal structures of TiO_2@SiO_2-g-EVMG nanohybrids

TiO_2@SiO_2-g-EVMG nanohybrids were prepared via a two-step reaction, i.e., i) KH550 was coupled to the surface of TiO_2@SiO_2 nanoparticles to form TiO_2@SiO_2–KH550 nanohybrids via the reaction between the hydroxyl groups of TiO_2@SiO_2 and the siloxane groups of KH550; ii) While for the second reaction between the –NH_2 groups of KH550 and the epoxy groups of EVMG (forming -N-C- covalent bond) is also well-known and it actually is the sole possible reaction in this process. These covalent grafting mechanisms have already been shown in Scheme 1. Then FT-IR, TGA and XRD were used to characterize their chemical and crystal structures, as shown in Fig. 3.

As shown in Fig. 3a–b, both TiO_2@SiO_2 and TiO_2@SiO_2-g-EVMG show FT-IR vibration peaks of Ti–O–Si and Si–O–Si bonds at 954 and 1071 cm^{-1} [36], [37]respectively, which are ascribed to the coated SiO_2 shell. Compared with TiO_2@SiO_2, the FT-IR spectrum of TiO_2@SiO_2--g-EVMG shows new stretching vibration peaks at 2800~3000 cm^{-1} and 1730 cm^{-1}, corresponding to the C–H bond and carbonyl groups of the grafted EVMG chains, respectively [38]. A direct evidence for the -N-C- covalent bond was not obtained due to its very low content and embedded inside by the grafted EVMG. However, the TiO_2@SiO_2--g-EVMG nanohybrids were carefully purified before any measurement to remove the free EVMG (i.e., without covalent bond to the nanoparticles). Therefore, the new stretching vibration peaks at 2800~3000 cm^{-1} and 1730 cm^{-1} can provide sufficient evidence to support the conclusion about the covalent bonding. The Photos of TiO_2@SiO_2 and TiO_2@SiO_2-g-EVMG in chloroform were shown in Fig. S1. The grafting degree of EVMG can be quantitatively characterized by TGA, as shown in Fig. 3c. TiO_2@SiO_2 is thermally stable with a mass loss of 3.4 wt% at 600 °C, whereas EVMG sharply decomposes at around 330 °C and 450 °C corresponding to the ester side-chain and the ethylene

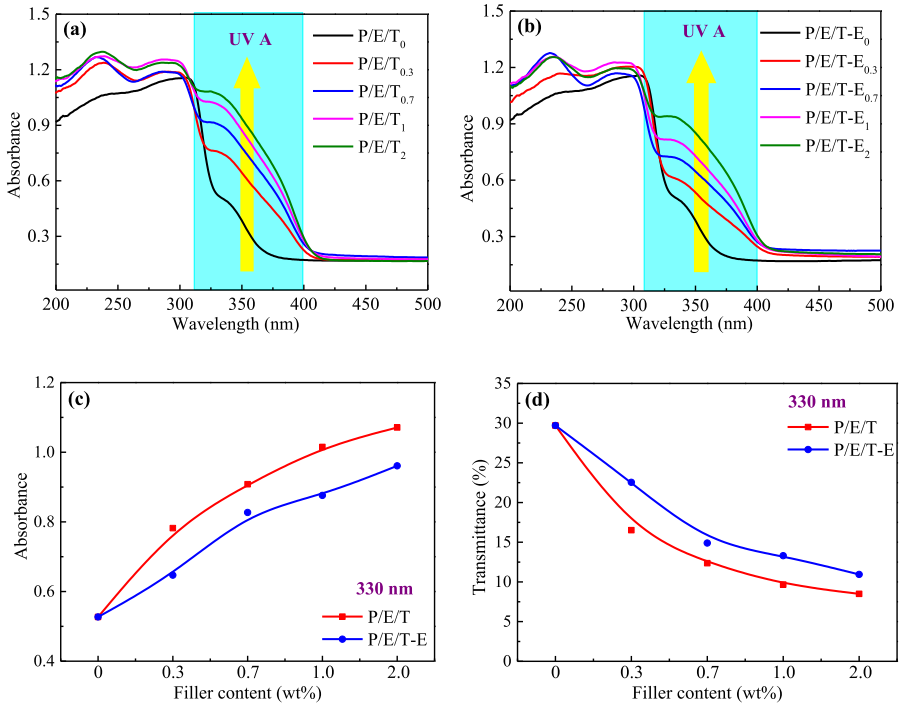

Fig. 4. UV–Vis absorption spectra of (a) P/E/T_x and (b) P/E/T-E_x nanocomposites with different content of nanofillers, (c) the UV absorption and transmittance values of P/E/T_x and P/E/T-E_x nanocomposites at 330 nm as a function of filler contents.

main-chain, respectively, and its final residual mass at 600 °C is almost 0. The mass loss of TiO_2@SiO_2-g-EVMG at 600 °C is 9.6 wt%. Apparently, the extra mass loss of TiO_2@SiO_2-g-EVMG compared with TiO_2@SiO_2 is ascribed to the decomposition of EVMG chains, i.e., the grafting degree of EVMG can be roughly calculated as around 6 wt% [39]. In addition, the TGA curves of PBT/EVMG (P/E) and PBT/EVMG/TiO_2@SiO_2-g-EVMG (P/E/T-E) composites were shown in Fig. S2. The TGA curve of P/E composites was almost coincided with that of P/E/T-E composites, indicating that thermal stability of PBT/EVMG materials were not affected obviously by incorporation of the TiO_2@SiO_2-g-EVMG nanohybrids.

Since the UV absorption performance of TiO_2 is strongly associated

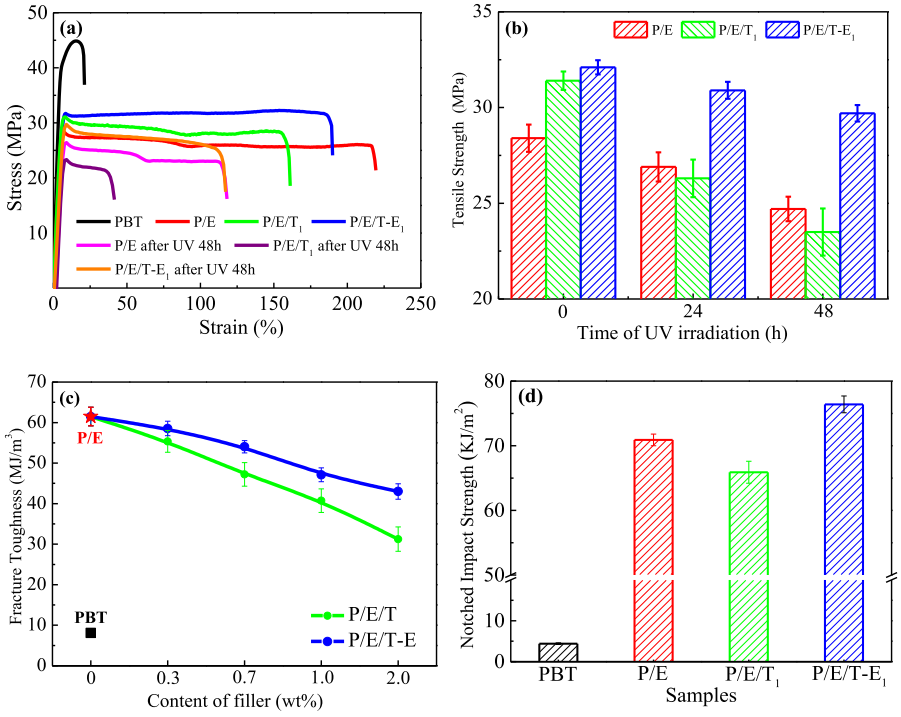

Fig. 5. (a) Stress-strain curves and (b) tensile strength of PBT composites before and after UV irradiation, (c) fracture toughness and (d) notch impact strength of PBT composites without UV irradiation.

Table 1
The mechanical properties of PBT composites before UV irradiation and the conservation percentage in mechanical properties after 48h UV irradiation.

Samples	σ (MPa)	$D_σ$ (%)	ε (%)	$D_ε$ (%)	Fracture toughness (MJ/m^3)
P/E	28.4 ± 0.7	87.7 ± 2.1	212 ± 9	62.3 ± 1.6	61.5 ± 2.3
P/E/$T_{0.3}$	29.3 ± 0.6	86.4 ± 2.3	187 ± 8	60.4 ± 1.4	55.4 ± 2.7
P/E/$T_{0.7}$	30.4 ± 0.6	81.2 ± 3.3	167 ± 8	51.5 ± 1.6	47.2 ± 2.9
P/E/T_1	31.4 ± 0.5	74.9 ± 3.8	135 ± 7	45.2 ± 1.8	40.7 ± 2.9
P/E/T_2	30.2 ± 0.8	69.4 ± 4.0	118 ± 8	41.5 ± 1.7	31.2 ± 3.0
P/E/T-$E_{0.3}$	29.4 ± 0.4	90.0 ± 1.3	193 ± 7	71.4 ± 1.2	58.5 ± 1.8
P/E/T-$E_{0.7}$	31.9 ± 0.5	91.1 ± 1.1	178 ± 6	76.1 ± 0.9	54.0 ± 1.5
P/E/T-E_1	32.1 ± 0.4	92.5 ± 1.2	161 ± 6	82.0 ± 0.8	47.1 ± 1.7
P/E/T-E_2	32.3 ± 0.6	95.0 ± 1.2	149 ± 4	86.6 ± 0.9	43.0 ± 1.9

with its crystal structures [40], the crystal structures of TiO_2, TiO_2@SiO_2 and TiO_2@SiO_2-g-EVMG are investigated by XRD, as shown in Fig. 3d. As reported, TiO_2 show typical characteristic diffraction peaks corresponding to 110, 101 and 211 crystalline planes [41]. In this study, the TiO_2@SiO_2 and TiO_2@SiO_2-g-EVMG exhibit the same diffraction signals as TiO_2. These results indicate that the crystal structures of TiO_2 did not change after coating with SiO_2 or SiO_2-g-EVMG, and thus the modified TiO_2 nanoparticles maintain high UV absorption ability, see discussion below.

3.3. UV-shielding properties of PBT nanocomposites with TiO_2@SiO_2-g-EVMG

TiO_2 as a functional additive in materials can strengthen their UV-shielding property and, as a result, protecting human body or objects from UV radiation. In this work, the UV-shielding behaviours of PBT with different types of TiO_2 nanoparticles were monitored by an UV–Vis near-infrared spectrophotometer, as shown in Fig. 4.

As shown in Fig. 4a and b, pure P/E exhibits the lowest UV absorption values in almost the whole region of UV light wavelength. Specifically, the absorption values of both P/E/T_x and P/E/T-E_x nanocomposites gradually increase in the UV-A region (320–400 nm) with increasing the TiO_2 or TiO_2@SiO_2-g-EVMG contents, which is ascribed to the inherent UV-absorbing character of TiO_2. Taking the wavelength of 330 nm as an example, the UV absorption values of the PBT nanocomposites as a function of filler content are shown in Fig. 4c. The UV transmittance of the material can be calculated according to the Lambert-Beer law A = -lgT (the A and T represent the light absorbance and light transmittance respectively [42]) and the results are shown in Fig. 4d. Actually, the UV transmittance can be corresponded to the percentage that UV light was shielded. In Figs. 4d and 30% of the UV light was shielded by the pure P/E material whereas about 90% of the UV light was shielded by PBT composites with 1.0–2.0 wt% TiO_2 and TiO_2@SiO_2-g-EVMG nanohybrids, demonstrating an obviously enhanced UV-shielding performance of PBT-based nanocomposites. It is worthy to note that, the UV-shielding performance of the PBT in the UV-B region (280–320 nm) has been also improved obviously in the presence of the TiO_2@SiO_2-g-EVMG.

3.4. UV resistance behaviors of PBT nanocomposites with TiO_2@SiO_2-g-EVMG

As discussed above, the issue of TiO_2-based polymeric nanocomposites is to address the problem of instability in UV-light due to the photocatalytic effect of TiO_2. Thus, the mechanical properties of the P/E/T and P/E/T-E nanocomposites as a function of accelerated UV irradiation were studied, as shown in Fig. 5 and Table 1. Neat PBT exhibits a tensile strength (σ) of ~45 MPa and an elongation at break (ε) of ~20% (Fig. 5a). The σ decreased to 28 MPa whereas the ε of P/E composites increased up to 210% due to the presence of rubbery EVMG component. After incorporation of 1 wt% TiO_2 and TiO_2@SiO_2-g-EVMG, the σ of P/E/T_1 and P/E/T-E_1 nanocomposites increased to 31 and 32 MPa, while the ε of P/E/T_1 and P/E/T-E_1 nanocomposites decreased to 135% and 160%, respectively (Fig. 5a/b). Obviously, both σ and ε of the P/E/T-E_1 nanocomposites are higher than those of the P/E/T_1 nanocomposites. The fracture toughness calculated by the stress-strain curves and the notched impacted strength show a similar trend (Fig. 5c/d). Moreover, the DSC measurements of P/E, P/E/T_1 and P/E/T-E_1 blends have been provided in Fig. S3 and the crystallinity degree of the matrix has been quantified as shown in Table S1. It can be seen that the crystallinity degree of the PBT matrix was not be affected by untreated and treated TiO_2, while the crystallization temperature was increased slightly.

The mechanical properties of all P/E, P/E/T and P/E/T-E composites decreased after 48 h UV irradiation, notably for the P/E/T_1 nanocomposites whose σ and ε remained only by 75% and 45%, respectively, due to the strong photocatalytic effect of TiO_2 nanoparticles. However, the mechanical properties of P/E/T-E nanocomposites are much more UV stable in comparison with the other two samples, e.g., the σ and the ε of P/E/T-E_1 nanocomposites remained by 93% and 82% respectively after 48 h irradiation. With increasing the content of TiO_2 nanoparticles, the UV resistance behaviour of PBT nanocomposites would be better. This interesting phenomenon is attributed to the weakened

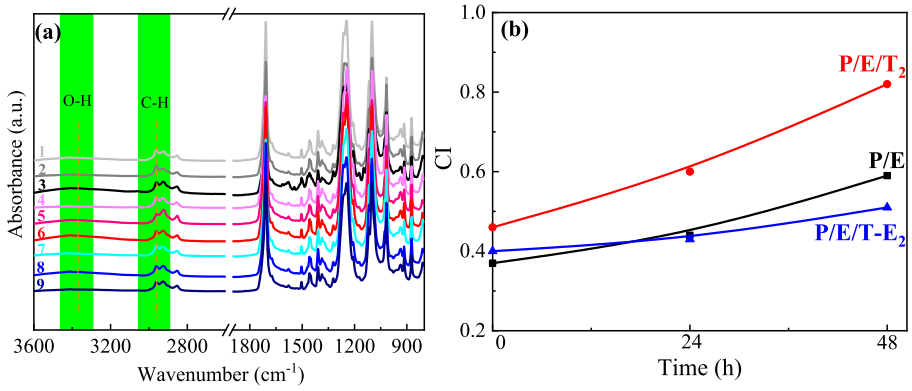

Fig. 6. (a) FT-IR spectra (wherein the samples 1, 2 and 3 represent the P/E blends after UV radiation for 0 h, 24 h and 48 h, respectively; 4, 5 and 6 represent the P/E/T_2 composites after UV radiation for 0 h, 24 h and 48 h, respectively; 7, 8 and 9 represent the P/E/T-E_2 composites after UV radiation for 0 h, 24 h and 48 h, respectively) and (b) carboxyl index (CI) of different PBT composites as a function of UV radiation time.

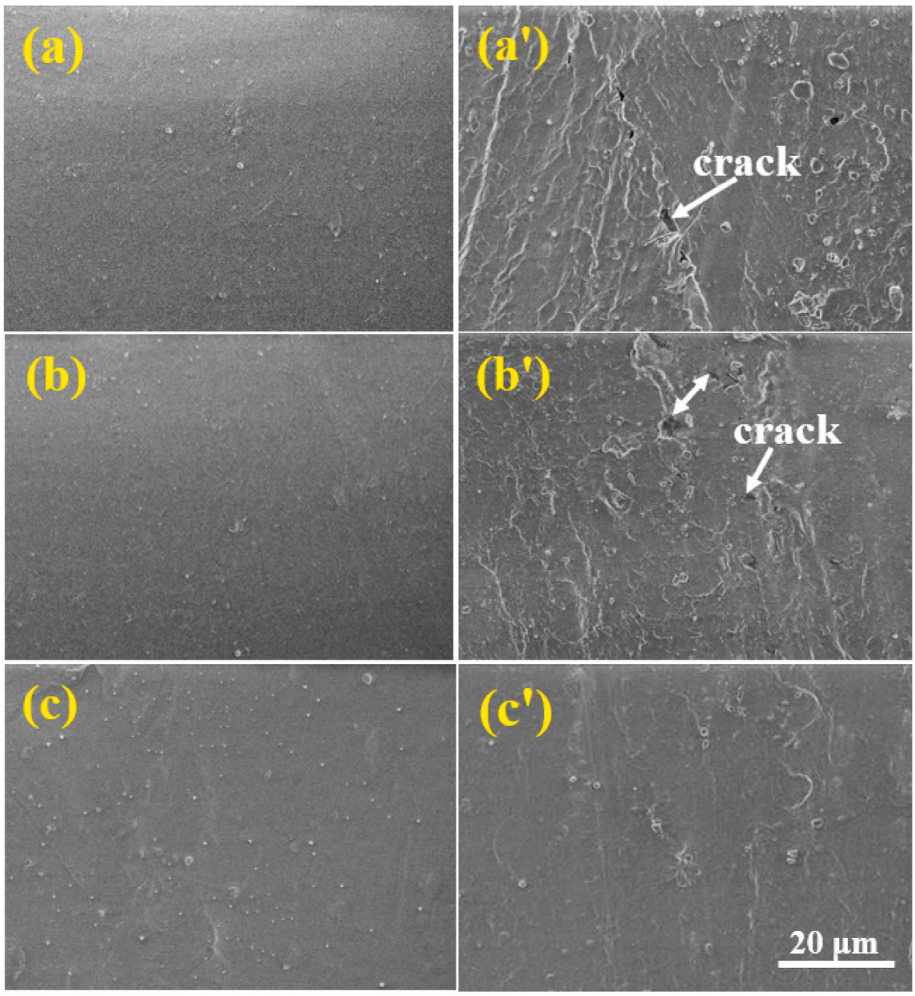

Fig. 7. SEM images of the surfaces of (a/a') P/E, (b/b') P/E/T_2 and (c/c') P/E/T-E_2 composites, wherein the (a/b/c) and (a'/b'/c') images are corresponding to the surfaces before and after UV irradiation, respectively.

photocatalytic activity of TiO_2@SiO_2-g-EVMG nanohybrids due to the coating of SiO_2-g-EVMG layers (see discussion in Section 3.1) and their selective distribution in EVMG phase only (see morphology discussion later).

Notes: σ, ε represent the tensile strength and elongation at break of PBT composites before UV irradiation, respectively. D_σ and D_ε represent the conservation percentage of σ and ε after 48 h UV irradiation, respectively.

In order to provide a deeper insight in the UV degradation behaviors, FT-IR was used to follow the change of the PBT molecular structure as a function of UV irradiation, as shown in Fig. 6. Cleavage of ester bonds occurred dominantly in the case of PET during photo-degradation and subsequently led to shorter polyester chains containing more terminal carboxyl groups, and deterioration in mechanical properties [43]. According to literatures [44,45], carboxyl index (CI) can be used to quantify the extent of PBT degradation, which is determined as the intensity ratio of peak 3290 cm^{-1} (assigned to the O–H vibration of –COOH groups) to the internal standard peak (2960 cm^{-1} corresponding to C–H vibration). It has to be mentioned that the FT-IR spectra have been shifted in Fig. 6 to avoid overlap. The CI values of each composite are shown in Fig. 6b as a function of UV irradiation time. After UV irradiation, the CI values for all P/E, P/E/T and P/E/T-E composites increased. However, the CI values of P/E/T-E nanocomposite increased slowly and are much lower than those of P/E and P/E/T composites. For example, the CI value of the P/E/T_2 nanocomposite increased from 0.40 to 0.82 after an 48 h UV irradiation, while the CI value of the P/E/T-E_2 nanocomposite increased only by 0.09, indicating that the cleavage of PBT ester bond was prevented significantly by the TiO_2@SiO_2-g-EVMG nanohybrids. It means that the core-shell structure of TiO_2@SiO_2--g-EVMG enhanced the UV stability of the P/E/T-E nanocomposites, which is well in accordance with the mechanical property discussion in Section 3.4.

SEM was further used to observe the surface morphology of P/E, P/E/T_2 and P/E/T-E_2 composites before and after UV irradiation, and the micro morphologies are shown in Fig. 7.

All the surfaces of P/E, P/E/T_2 and P/E/T-E_2 composites are smooth and flat before UV irradiation (Fig. 7a/b/c). After 48 h of accelerated UV irradiation, the surface of the P/E composite became rough and some small cracks are visible (Fig. 7a'). In comparison with P/E composite, the P/E/T_2 nanocomposite exhibited rougher surface and larger cracks (Fig. 7b') due to the photo-degradation acceleration effect of TiO_2 under UV irradiation. However, the P/E/T-E_2 nanocomposite shows a certain extent of UV resistance as confirmed by the relatively smooth surface after UV irradiation (Fig. 7c'). Obviously, the SEM results are consistent with the above mechanical and FT-IR data. Therefore, it can be concluded that super-toughened PBT nanocomposites with both superior UV shielding and UV resistance can be obtained via incorporation of the core-shell structured TiO_2 @SiO_2-g-EVMG nanohybrids.

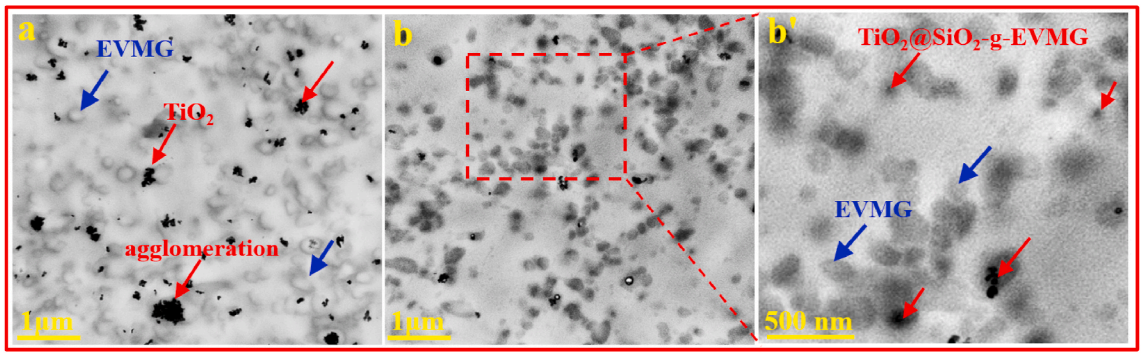

Fig. 8. TEM images of (a) P/E/T_1 and (b/b') P/E/T-E_1 nanocomposites. The EVMG phase, TiO_2 and TiO_2@SiO_2-EVMG nanohybrids are marked with blue and red arrows, respectively, showing that TiO_2 aggregates were dispersed in both PBT and EVMG phases while the TiO_2@SiO_2-EVMG were selectively dispersed in the EVMG phase. (For interpretation of the references to colour in this figure legend, the reader is referred to the Web version of this article.)

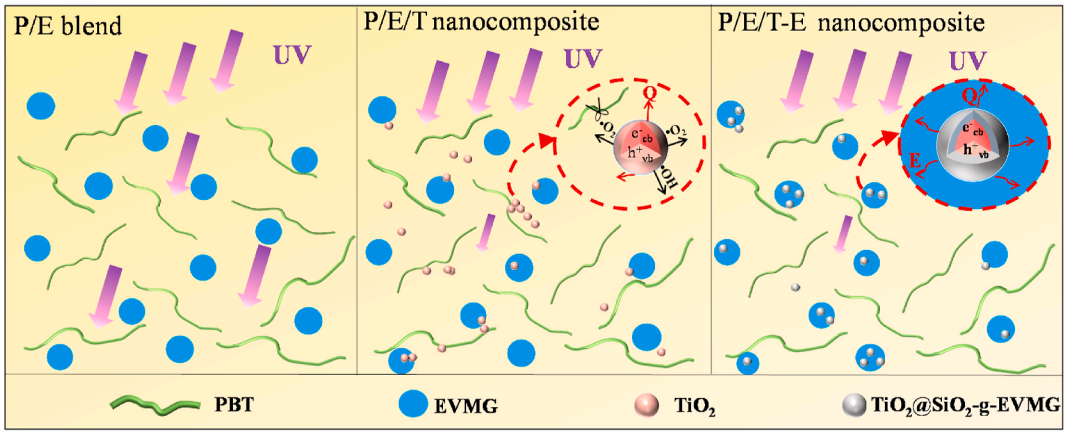

Fig. 9. Schematic diagram of UV resistance mechanism of PBT nanocomposites (Where, the Q and E represent the emitted heat and electromagnetic energy, respectively).

3.5. Toughening and UV resistance mechanisms of the P/E/T-E nanocomposites

The morphology of P/E/T and P/E/T-E nanocomposites was investigated in more details by TEM, as shown in Fig. 8. Spherical-like EVMG particles with a dimension of 200–300 nm are dispersed uniformly in both P/E/T and P/E/T-E nanocomposites. In addition, neat TiO_2 nanoparticles randomly agglomerated in both PBT and EVMG phases, and the size can be as large as 500 nm (Fig. 8a). In the presence of external stress, the TiO_2 aggregates are easier to serve as the stress concentrators to generate large cracks and make the material fail. However, the TiO_2@SiO_2-g-EVMG nanohybrids were more uniformly and selectively dispersed in the EVMG phase with an average size of 200 nm due to the surface-grafted EVMG chains (Fig. 8b/b'), indicating a better affinity between the TiO_2@SiO_2-g-EVMG nanohybrids and the EVMG phase. Thus, the P/E/T-E nanocomposite exhibited a better facture toughness.

As known, TiO_2 nanoparticles could endow polymer materials with excellent UV shielding properties (as seen in Fig. 4), thus making it possible for P/E/T and P/E/T-E nanocomposites to prevent UV lights penetrating the composites. In other words, the degradation behaviors caused by UV radiation may dominantly occur on the surface or on the top layer of the nanocomposites. In the meantime, the TiO_2 nanoparticles in P/E/T would create free radicals after absorbing UV energy, and then directly attack the PBT matrix. The photocatalytic degradation effect of TiO_2 is greater than the UV shielding protection, thus leading to a poor UV resistance of P/E/T nanocomposite. However, in the P/E/T-E nanocomposite, the SiO_2-shell and the selective dispersion of TiO_2@SiO_2-g-EVMG nanohybrids in the EVMG phase prevent a direct contact between TiO_2 and PBT matrix, and the UV energy absorbed by TiO_2@SiO_2-g-EVMG nanohybrids eventually dissipated by heat or electromagnetic energy [46] (as seen in Fig. 9). Combined with the UV shielding properties of top layer of P/E/T-E nanocomposites and the weakened photocatalytic effect of TiO_2@SiO_2-g-EVMG nanohybrids, it finally resulted in a considerable improvement in the UV resistance of the P/E/T-E nanocomposites.

4. Conclusion

PBT including recycled PBT materials suffer from brittleness and UV instability. In this work, PBT nanocomposites with superior toughness and UV resistance are achieved by compounding with both epoxidized elastomer (EVMG) and tailor-made TiO_2@SiO_2-g-EVMG nanohybrids. The TiO_2@SiO_2-g-EVMG nanohybrids were designed via covalent grafting modifications and their structure was confirmed by TEM and FT-IR characterization. The morphology of PBT/EVMG/TiO_2@SiO_2-g-EVMG nanocomposites demonstrated that the EVMG chains grafted on the surface of TiO_2@SiO_2-g-EVMG nanohybrids were conducive to a uniform and selective dispersion of the nanohybrids in EVMG phase only. Furthermore, the selective dispersion of TiO_2@SiO_2-g-EVMG nanohybrids and the coated SiO_2 shell avoid the direct contact of TiO_2 and PBT matrix, which further prevents the free radicals that initiated by TiO_2 from attacking the PBT matrix, thus resulting in excellent UV resistance of the PBT/EVMG/TiO_2@SiO_2-g-EVMG nanocomposites. In addition, the TiO_2@SiO_2-g-EVMG nanohybrids also obviously enhanced the UV-shielding property and reinforced the PBT-based nanocomposites. Therefore, this work provides a new route to make robust

PBT nanocomposites with both superior UV resistance and UV shielding performances, and it may broaden the application of PBT in more advanced and durable applications including PBT/PC blends.

CRediT authorship contribution statement

Ying Cao: Writing - original draft, Formal analysis, Data collection, and analysis. **Pengwu Xu:** Writing - original draft, Formal analysis, Data collection, and analysis. **Weijun Yang:** Investigation, Formal analysis. **Xiangmiao Zhu:** Investigation, Formal analysis. **Weifu Dong:** Writing - original draft. **Mingqing Chen:** Writing - original draft. **Mingliang Du:** Data collection, and analysis, Writing - original draft. **Tianxi Liu:** Data collection, and analysis, Writing - original draft. **Pieter Jan Lemstra:** Investigation, Formal analysis. **Piming Ma:** Conceptualization, Supervision, Writing - review & editing.

Declaration of competing interest

The authors declare that they have no known competing financial interests or personal relationships that could have appeared to influence the work reported in this paper.

Acknowledgements

This work is supported by the National Natural Science Foundation of China (51873082, 52073123) and the MOE & SAFEA 111 Project (B13025). The authors also would like to acknowledge Dr. Theo Hoeks (SABIC Europe) for their valuable contributions.

Appendix A. Supplementary data

Supplementary data to this article can be found online at https://doi.org/10.1016/j.compositesb.2020.108510.

References

[1] Sasanuma Y, Wagai Y, Suzuki N, Abe D. Conformational characteristics and configurational properties of poly (butylene terephthalate) and structure-property relationships of aromatic polyesters. Polymer 2013;54:3904–13. https://doi.org/10.1016/j.polymer.2013.05.044.

[2] Zhu JH, Cai JL, Xie WC, Chen PH, Gazzano M, Scandola M, et al. Poly(butylene 2,5-furan dicarboxylate), a biobased alternative to PBT: synthesis, physical properties, and crystal structure. Macromolecules 2013;46:796–804. https://doi.org/10.1021/ma3023298.

[3] Fu N, Li G, Zhang Q, Wang N, Qu X. Preparation of a functionalized core-shell structured polymer by seeded emulsion polymerization and investigation on toughening poly (butylene terephthalate). RSC Adv 2014;4:1067–73. https://doi.org/10.1039/C3RA44163F.

[4] Gijsman P, Meijers G, Vitarelli G. Comparison of the UV-degradation chemistry of polypropylene, polyethylene, polyamide 6 and polybutylene terephthalate. Polym Degrad Stabil 1999;65:433–41. https://doi.org/10.1016/S0141-3910(99)00033-6.

[5] Müller U, Rätzsch M, Schwanninger M, Steiner M, Zöbl H. Yellowing and IR-changes of spruce wood as result of UV-irradiation. J Photochem Photobiol, B 2003;69:97–105. https://doi.org/10.1016/S1011-1344(02)00412-8.

[6] Turton T, White J. Effect of stabilizer and pigment on photo-degradation depth profiles in polypropylene. Polym Degrad Stabil 2001;74:559–68. https://doi.org/10.1016/S0141-3910(01)00193-8.

[7] Yang L, Chen H, Jia S, Lu X, Huang J, Yu X, et al. Influences of ethylene-butylacrylate-glycidyl methacrylate on morphology and mechanical properties of poly (butylene terephthalate)/polyolefin elastomer blends. J Appl Polym Sci 2014;131. https://doi.org/10.1002/app.40660.

[8] Deng S, Bai H, Liu Z, Zhang Q, Fu Q. Toward supertough and heat-resistant stereocomplex-type polylactide/elastomer blends with impressive melt stability via in situ formation of graft copolymer during one-pot reactive melt blending. Macromolecules 2019;52:1718–30. https://doi.org/10.1021/acs.macromol.8b02626.

[9] Wu B, Zeng Q, Niu D, Yang W, Dong W, Chen M, et al. Design of supertoughened and heat-resistant PLLA/elastomer blends by controlling the distribution of stereocomplex crystallites and the morphology. Macromolecules 2019;52:1092–103. https://doi.org/10.1021/acs.macromol.8b02262.

[10] Cao Y, Xu P, Wu B, Hoch M, Lemstra PJ, Yang W, et al. High-performance and functional PBT/EVMG/CNTs nanocomposites from recycled sources by in situ multistep reaction-induced interfacial control. Compos Sci Technol 2020;190:108043. https://doi.org/10.1016/j.compscitech.2020.108043.

[11] Liu G, He Y, Zeng J, Li Q, Wang Y. Fully biobased and supertough polylactide-based thermoplastic vulcanizates fabricated by peroxide-induced dynamic vulcanization and interfacial compatibilization. Biomacromolecules 2014;15:4260–71. https://doi.org/10.1021/bm5012739.

[12] Chen Y, Yuan D, Xu C. Dynamically vulcanized biobased polylactide/natural rubber blend material with continuous cross-linked rubber phase. ACS Appl Mater Interfaces 2014;6:3811–6. https://doi.org/10.1021/am5004766.

[13] Xu C, Fan J, Yuan D, Wang Y, Chen Y. Model construction of particle size in dynamic vulcanization of PVDF/SR blends-matching degree between crosslinking and shearing rates. Mater Chem Phys 2019;222:200–6. https://doi.org/10.1016/j.matchemphys.2018.10.011.

[14] Moffett A, Dekkerrs M. Compatibilized and dynamically vulcanized thermoplastic elastomer blends of poly (butylene terephthalate) and ethylene propylene diene rubber. Polym Eng Sci 1992;32:1–5. https://doi.org/10.1002/pen.760320102.

[15] Li JL, Wang XF, Yang CJ, Yang JH, Wang Y, Zhang JH. Toughening modification of polycarbonate/poly(butylene terephthalate) blends achieved by simultaneous addition of elastomer particles and carbon nanotubes. Compos. Part A-Appl S 2016;90:200–10. https://doi.org/10.1016/j.compositesa.2016.07.006.

[16] Chen Y, Wang W, Qiu Y, Li L, Qian L, Xin F. Terminal group effects of phosphazene-triazine bi-group flame retardant additives in flame retardant polylactic acid composites. Polym. Degrad. Stabil. 2017;140:166–75. https://doi.org/10.1016/j.polymdegradstab.2017.04.024.

[17] Zeng Q, Ma P, Su X, Lai D, Zeng X, Li H. Facile fabrication of superhydrophobic and magnetic poly (lactic acid) non-woven fabric for oil-water separation. Ind Eng Chem Res 2020;59:9127–35. https://doi.org/10.1021/acs.iecr.0c01033.

[18] Xu P, Lv P, Wu B, Ma P, Dong W, Chen M, et al. Smart design of rapid crystallizing and non-leaching antibacterial poly(lactide) nanocomposites by sustainable aminolysis grafting and in situ interfacial stereocomplexation. ACS Sustain Chem Eng 2018;6:13367–77. https://doi.org/10.1021/acssuschemeng.8b03131.

[19] Liu Y, Cao L, Yuan D, Chen Y. Design of super-tough co-continuous PLA/NR/SiO_2 TPVs with balanced stiffness-toughness based on reinforced rubber and interfacial compatibilization. Compos Sci Technol 2018;165:231–9. https://doi.org/10.1016/j.compscitech.2018.07.005.

[20] Yang W, Weng Y, Puglia D, Qi G, Dong W, Kenny JM, et al. Poly(lactic acid)/lignin films with enhanced toughness and anti-oxidation performance for active food packaging. Int J Biol Macromol 2020;144:102–10. https://doi.org/10.1016/j.ijbiomac.2019.12.085.

[21] Zhang Z, Wang S, Zhang J, Zhu W, Zhao X, Tian T, et al. Self-formation of elastomer network assisted by nano-silicon dioxide particles: a simple and efficient route toward polymer nanocomposites with simultaneous improved toughness and stiffness. Chem Eng J 2016;285:439–48. https://doi.org/10.1016/j.cej.2015.09.066.

[22] Huang J, Cao L, Yuan D, Chen Y. Design of novel self-healing thermoplastic vulcanizates utilizing thermal/magnetic/light-triggered shape memory effects. ACS Appl Mater Interfaces 2018;10:40996–1002. https://doi.org/10.1021/acsami.8b18212.

[23] Man C, Zhang C, Liu Y, Wang W, Ren W, Jiang L, et al. Poly(lactic acid)/titanium dioxide composites: preparation and performance under ultraviolet irradiation. Polym Degrad Stabil 2012;97:856–62. https://doi.org/10.1016/j.polymdegradstab.2012.03.039.

[24] Xiu H, Qi X, Bai H, Zhang Q, Fu Q. Simultaneously improving toughness and UV-resistance of polylactide/titanium dioxide nanocomposites by adding poly(ether) urethane. Polym Degrad Stabil 2017;143:136–44. https://doi.org/10.1016/j.polymdegradstab.2017.07.002.

[25] Zhou S, Wang F, Balachandran S, Li G, Zhang X, Wang R, et al. Facile fabrication of hybrid PA6-decorated TiO_2 fabrics with excellent photocatalytic, anti-bacterial, UV light-shielding, and super hydrophobic properties. RSC Adv 2017;7:52375–81. https://doi.org/10.1039/C7RA09613E.

[26] Huang JY, Li SH, Ge MZ, Wang LN, Xing TL, Chen GQ, et al. Robust superhydrophobic TiO_2@fabrics for UV shielding, self-cleaning and oil-water separation. J Mater Chem A 2015;3:2825–32. https://doi.org/10.1039/c4ta05332j.

[27] Li C, Li Z, Ren X. Preparation and characterization of polyester fabrics coated with TiO_2/benzotriazole for UV protection. Colloid Surface A 2019;577:695–701. https://doi.org/10.1016/j.colsurfa.2019.06.030.

[28] Xiao X, Liu X, Chen F, Fang D, Zhang C, Xia L, et al. Highly anti-UV properties of silk fiber with uniform and conformal nanoscale TiO_2 coatings via atomic layer deposition. ACS Appl Mater Interfaces 2015;7:21326–33. https://doi.org/10.1021/acsami.5b05868.

[29] Xuan L, Han G, Wang D, Cheng W, Gao X, Chen F, et al. Effect of surface-modified TiO_2 nanoparticles on the anti-ultraviolet aging performance of foamed wheat straw fiber/polypropylene composites. Materials 2017;10:456. https://doi.org/10.3390/ma10050456.

[30] Nakayama N, Hayashi T. Preparation and characterization of poly(l-lactic acid)/TiO_2 nanoparticle nanocomposite films with high transparency and efficient photodegradability. Polym Degrad Stabil 2007;92:1255–64. https://doi.org/10.1016/j.polymdegradstab.2007.03.026.

[31] Zan L, Fa W, Wang S. Novel photodegradable low-density polyethylene-TiO_2 nanocomposite film. Environ Sci Technol 2006;40:1681–5. https://doi.org/10.1021/es051173x.

[32] Buzarovska A, Grozdanov A. Biodegradable poly(L-lactic acid)/TiO_2 nanocomposites: thermal properties and degradation. J Appl Polym Sci 2012;123. https://doi.org/10.1002/app.34729.

[33] Zhang Y, Xu H, Xu Y, et al. The effect of lanthanide on the degradation of RB in nanocrystalline Ln/TiO_2 aqueous solution. J Photochem Photobiol, A 2005;170:279–85. https://doi.org/10.1016/j.jphotochem.2004.09.001.

[34] Wang KH, Hsieh YH, Chen LJ. The heterogeneous photocatalytic degradation, intermediates and mineralization for the aqueous solution of cresols and nitrophenols. J Hazard Mater 1998;59:251–60. https://doi.org/10.1016/s0304-3894(97)00151-9.

[35] Fatima R, Afridi MN, Kumar V, Lee J, Ali I, Kim KH, et al. Photocatalytic degradation performance of various types of modified TiO_2 against nitrophenols in aqueous systems. J Clean Prod 2019;231:899–912. https://doi.org/10.1016/j.jclepro.2019.05.292.

[36] Furusawa T, Honda K, Ukaji E, et al. The microwave effect on the properties of silica-coated TiO_2 fine particles prepared using sol-gel method. Mater Res Bull 2008;43:946–57. https://doi.org/10.1016/j.materresbull.2007.04.031.

[37] Cheng F, Sajedin SM, Kelly SM, Lee AF, Kornherr A. UV-stable paper coated with APTES-modified P25 TiO_2 nanoparticles. Carbohydr Polym 2014;114:246–52. https://doi.org/10.1016/j.carbpol.2014.07.076.

[38] Choi EY, Kim SW, Kim CK. In situ grafting of polybutylene terephthalate onto multi-walled carbon nanotubes by melt extrusion, and characteristics of their composites with polybutylene terephthalate. Compos Sci Technol 2016;132:101–7. https://doi.org/10.1016/j.compscitech.2016.07.003.

[39] Xu P, Yang W, Niu D, Yu M, Du M, Dong W, et al. Multifunctional and robust polyhydroxyalkanoate nanocomposites with superior gas barrier, heat resistant and inherent antibacterial performances. Chem Eng J 2020;382:122864. https://doi.org/10.1016/j.cej.2019.122864.

[40] Gang L, Wang X, Chen Z, Cheng HM, Lu GQ. The role of crystal phase in determining photocatalytic activity of nitrogen doped TiO_2. J Colloid Interface Sci 2009;329:331–8. https://doi.org/10.1016/j.jcis.2008.09.061.

[41] Chen G, Ji S, Sang Y, Chang S, Wang Y, Hao P, et al. Synthesis of scaly Sn_3O_4/TiO_2 nanobelt heterostructures for enhanced UV-visible light photocatalytic activity. Nanoscale 2015;7:3117–25. https://doi.org/10.1039/C4NR05749J.

[42] Haaland DM, Easterling RG, Vopicka DA. Multivariate least-squares methods applied to the quantitative spectral analysis of multicomponent samples. Appl Spectrosc 1985;39:73–84. https://doi.org/10.1366/0003702854249376.

[43] Day M, Wiles DM. Photochemical degradation of poly(ethylene terephthalate). III. Determination of decomposition products and reaction mechanism. J Appl Polym Sci 1972;16:203–15. https://doi.org/10.1002/app.1972.070160118.

[44] Fechine GJM, Rabello MS, Maior RMS. Surface characterization of photodegraded poly(ethylene terephthalate): the effect of ultraviolet absorbers. Polymer 2004;45:2303–8. https://doi.org/10.1016/j.polymer.2004.02.003.

[45] Blais P, Day M, Wiles DM. Photochemical degradation of poly(ethylene terephthalate). IV. Surface changes. J Appl Polym Sci 1973;17:1895–907. https://doi.org/10.1002/app.1973.070170622.

[46] Carneiro JO, Teixeira V, Nascimento JHO, Neves J, Tavares PB. Photocatalytic activity and UV-protection of TiO_2 nanocoatings on poly(lactic acid) fibres deposited by pulsed magnetron sputtering. J Nanosci Nanotechnol 2011;11:8979–85. https://doi.org/10.1166/jnn.2011.3514.